第 44 卷 第 9 期/2024 年 5 月/光学学报 研究论文

光学学报

不同掺杂浓度Lu掺杂GaN电子结构和光学性质的第一性原理研究

付莎莎，肖清泉*，唐华著，姚云美，邹梦真，叶建峰，谢泉
贵州大学大数据与信息工程学院新型光电子材料与技术研究所，贵州 贵阳 550025

摘要 采用密度泛函理论下的第一性原理平面波超软赝势方法，计算了本征GaN和不同Lu掺杂浓度（原子数分数）$Ga_{1-x}Lu_xN$（x=0.0625、0.125、0.1875、0.25）体系的电子结构和光学性质，研究了掺杂浓度为12.5%和18.75%时相同掺杂量下不同空间有序占位体系结构的稳定性。计算结果表明：掺杂后体系晶格参数均有所增大，Lu的掺入诱导了浅能级杂质，使掺杂后体系带隙较本征带隙（3.40 eV）小；与本征GaN相比，掺杂体系的静介电常数均增加，当掺杂浓度为25%时，静介电常数增大为5.42，介电函数虚部和吸收谱往低能方向移动，发生了红移现象，吸收光谱范围增大，最终GaN的光催化性能得到提升。

关键词 材料；氮化镓；替位掺杂；电子结构；光学性质
中图分类号 O471 **文献标志码** A **DOI**: 10.3788/AOS231938

1 引 言

作为第三代宽带隙半导体材料，III-V族化合物氮化镓具有3.40 eV的直接宽带隙[1-2]，具有较高的饱和电子漂移速度、高热导率、高击穿电压、耐高温和化学稳定性好等优点[3-5]，因此其在光电和电子器件[如发光二极管[6-7]、激光二极管[8-9]、高电子迁移率晶体管（HEMTs）[10-11]、紫外光电探测器[12-15]等]方面的应用引起了研究人员的广泛关注。GaN带隙大，这限制了其对可见光的响应，光催化活性低[16-18]。因此，越来越多的学者致力于对掺杂GaN的研究以提高其对可见光的利用率。实验研究方面：Arakawa等[19]研究发现基于PSD（pulse sputtering deposition）制备的硅掺杂氮化镓是一种很有前途的氮化镓基光学器件外延透明电极材料；唐道胜等[20]发现在绝缘C掺杂基片上生长的GaN薄膜具有优良的输运和光学性能；Ho等[21]研究发现在采用MOCVD（metal-organic chemical vapor deposition）技术生长的GaN∶Er外延层中实现电泵激光用于高功率半导体激光器是可行的；胡磊等[22]通过优化蓝光激光器p-AlGaN限制层的外延生长温度和设计量子阱结构，研制出了高功率蓝光激光器。Tetsuo等[23-24]在实验上使用MOCVD方法，通过精确控制气态源的流量和通断时间来控制外延层组分和掺杂浓度；Polyakov等[25-26]研究了Fe掺杂GaN材料的光电性质；Zeng等[27]通过在硅衬底上垂直集成GaN纳米线阵列和单层石墨烯，制备了基于石墨烯/GaN异质结的单片集成紫外-红外（UV-IR）双色光电探测器。理论研究方面：Maskar等[28]研究发现稀土元素（Pm、Sm、Eu）掺杂GaN在紫外可见光中的光吸收系数增大，透光率达到80%；Eisa[29]通过计算发现Cd共掺杂GaN使得带隙减小，光学性能得到了提高；Lantri等[30]研究发现GaN∶Er化合物适合于紫外光谱中的不同应用；Khan等[31-32]发现非金属元素和金属元素共掺入GaN后，其带隙变小且光催化活性得到提高。

随着研究的深入，各种稀土元素掺杂GaN的研究相继被报道。稀土元素由于含有未充满的4*f*亚层，随着4*f*亚层中电子数的不断改变，稀土离子表现出不同形式的电子跃迁及十分丰富的能级跃迁[33-37]。稀土元素掺杂有望改善GaN可见光吸收，本研究利用第一性原理，研究了不同掺杂浓度下Lu掺杂GaN的电子结构和光学性质，计算结果为稀土元素Lu掺杂GaN半导体光电材料的器件开发提供理论支持。

2 计算模型和方法

2.1 计算方法

为了使计算结果更为准确，对超胞体系进行截断

收稿日期：2023-12-15；**修回日期**：2024-02-05；**录用日期**：2024-02-23；**网络首发日期**：2024-03-13
基金项目：贵州大学智能制造产教融合创新平台及研究生联合培养基地建设项目（2020-520000-83-01-324061）、贵州省留学回国人员科技活动择优资助项目（[2018]09）、贵州省高层次创新型人才培养项目（[2015]4015）
通信作者：*qqxiao@gzu.edu.cn

能和K点收敛测试。对300~700 eV的能量区间采用每间隔50 eV的计算方法进行测试，得到的结果如图1(a)所示。可以看出：当截断能E_{cut}=450 eV时能量曲线逐渐趋于平稳，故选取截断能为450 eV，以保证本研究计算的精确性。不同参数设置的K点测试结果如图1(b)所示，可以看出：当K点大小为4×4×2时，能量曲线逐渐趋于平稳，故选取该K点进行计算。

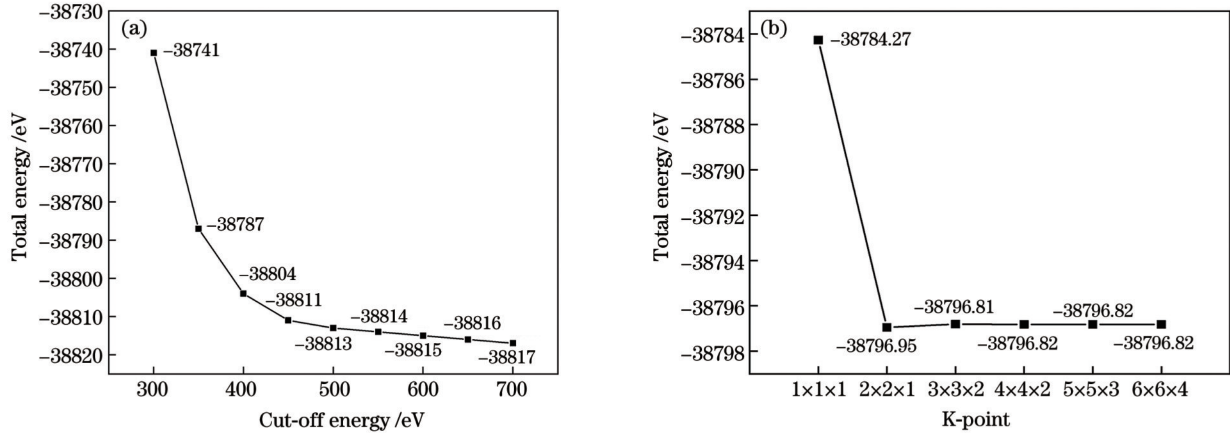

图1 截断能和K点收敛性测试结果。(a)截断能；(b) K点收敛性

Fig. 1 Test results of cut-off energy and K-point convergence. (a) Cut-off energy; (b) K-point convergence

基于密度泛函理论，采用CASTEP软件包[38]进行计算。本研究采用GGA+U平面波超赝势方法来修正带隙，U值(Hubbard参数)的选取参考Zakrzewski等[39-40]的结论。计算中，Ga、N、Lu原子的价电子分别为$3d^{10}4s^2 4p^1$、$2s^2 2p^3$、$4f^{14}5d^1 6s^2$。计算时选用广义梯度近似(GGA)和交换关联函数(PBE)来处理电子间相互作用的关联能，布里渊区积分采用MonkLurst-Pack[41]形式，取K点大小为4×4×2，单原子能量的收敛标准为1×10^{-5} eV/atom，自洽收敛精度为2×10^{-6} eV/atom，内应力为0.05 GPa，原子的最大位移收敛标准为0.001 Å。

2.2 计算模型

本研究采用的GaN纤锌矿结构属于P63mc空间群，晶格参数$a=b=0.3189$ nm，$c=0.5185$ nm，$c/a\approx1.626$，$\alpha=\beta=90°$，$\gamma=120°$。如图2所示，考虑到GaN的对称性，计算时分别构建了2×2×2的超晶胞模型、一个Lu原子替换一个Ga原子的$Ga_{0.9375}Lu_{0.0625}N$超胞结构、两个Lu替换两个Ga原子的5种相同掺杂浓度不同空间有序占位的$Ga_{0.875}Lu_{0.125}N$超胞模型、掺杂浓度为25%时3个Lu替换3个Ga原子的6种相同掺杂浓度不同空间有序占位的$Ga_{0.8125}Lu_{0.1875}N$超胞模型。考虑到4个Lu替换4个Ga原子的空间结构众多，本研究为节约计算资源，未考虑该类掺杂结构，只构建一种$Ga_{0.75}Lu_{0.25}N$超胞进行计算分析。

3 计算结果与分析

3.1 稳定性分析

为保证计算的准确性，计算前先对掺杂前后体系进行几何结构优化，所得参数见表1，a、b、c为体系的晶格参数，V为体积，E为总能，E_f为形成能，E_b为结合能。由表1可知，本征GaN优化后的c/a=1.624与实验值1.626吻合得较好，可见本研究计算方法可靠。不同掺杂浓度的Lu掺杂GaN体系的晶格常数和体积均大于本征体系，这主要是因为Lu^{3+}离子半径为0.085 nm，大于Ga^{3+}离子的半径(0.062 nm)[42]，Lu掺杂导致超晶胞晶格参数有所增大。形成能和结合能可以表征体系的稳定性和掺杂难易程度，形成能E_f和结合能E_b[43]分别满足

$$E_f = E_{doped} - E_{GaN} - n\mu_{Lu} + m\mu_{Ga}, \tag{1}$$

$$E_b = \frac{1}{N}\left(E_{doped} - E_{sum}\right), \tag{2}$$

式中：E_{doped}是Lu掺杂后GaN体系的总能量；E_{GaN}是未掺杂体系的总能量；μ_{Lu}和μ_{Ga}分别为Lu和Ga的原子化学势；n为掺杂Lu原子的个数；m为替换Ga原子的个数；N为体系内的原子总数；E_{sum}是体系内所有原子能量的总和。形成能越小，则掺杂越容易，结合能越小，体系越稳定。通过表1中形成能和结合能的对比可知，除$Ga_{0.9375}Lu_{0.0625}N$体系的形成能较高外，其他掺杂体系的形成能和结合能均为负值，这表明Lu掺杂的GaN体系结构具有稳定性。相比于其他掺杂体系，$Ga_{0.9375}Lu_{0.0625}N$体系的形成能为正值，这是由于：6.25%掺杂浓度的Lu相比于其他掺杂浓度Lu的掺入在GaN体系内与N离子的相互作用更强，造成了晶格畸变，使得能量升高，这一现象与Xiong等[44]的研究类似。两个Lu原子替换两个Ga原子的5种相同掺杂浓度、不同空间有序占位的$Ga_{0.875}Lu_{0.125}N$超胞结构中，结构2更稳定，相较于另外4种结构更容易实现掺杂；当掺杂浓度为18.75%时$Ga_{0.8125}Lu_{0.1875}N$的6种结构中，结构5相比于其他5种结构更为稳定，故下文就以$Ga_{0.875}Lu_{0.125}N$结构2和$Ga_{0.8125}Lu_{0.1875}N$结构5来讨论掺杂浓度为

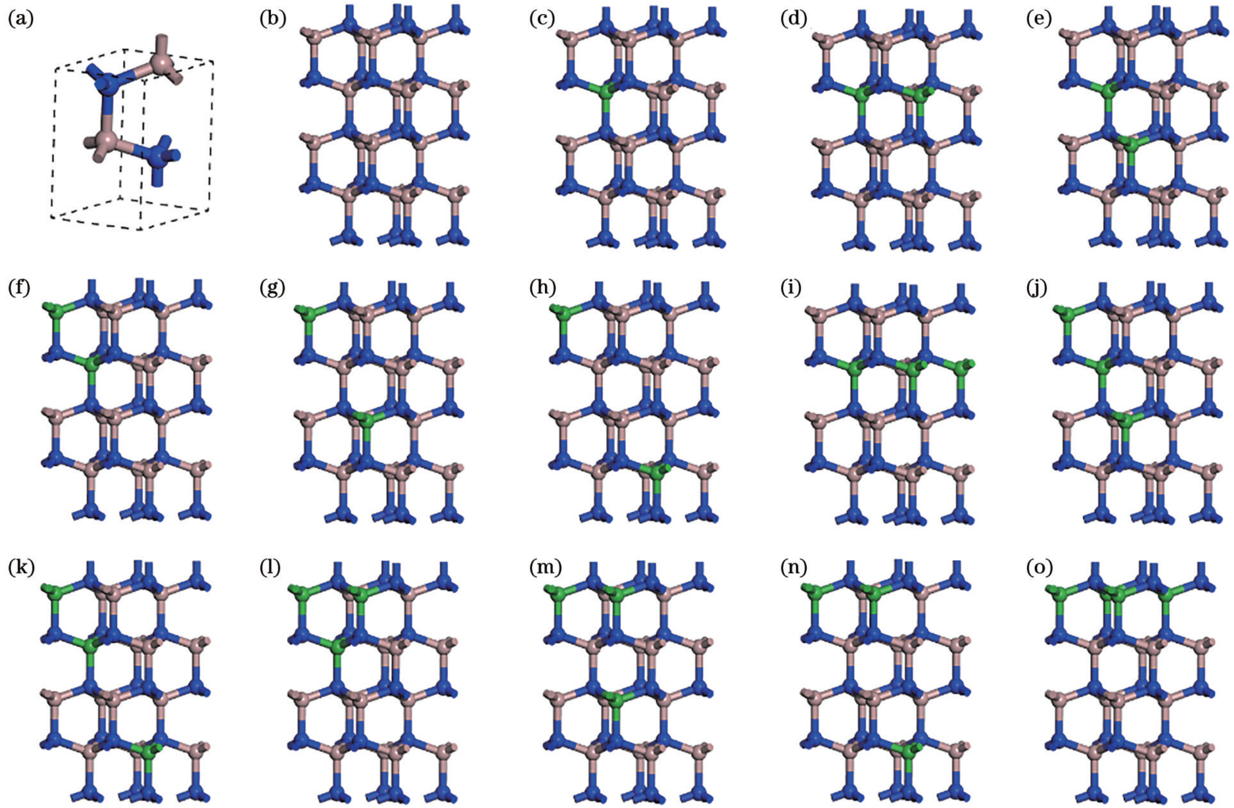

图2　超胞结构模型(其中蓝色为N原子,棕色为Ga原子,绿色为掺杂的Lu原子)。(a) GaN原胞;(b) GaN超胞;(c) $Ga_{0.9375}Lu_{0.0625}N$;(d) $Ga_{0.875}Lu_{0.125}N$ 结构1;(e) $Ga_{0.875}Lu_{0.125}N$ 结构2;(f) $Ga_{0.875}Lu_{0.125}N$ 结构3;(g) $Ga_{0.875}Lu_{0.125}N$ 结构4;(h) $Ga_{0.875}Lu_{0.125}N$ 结构5;(i) $Ga_{0.8125}Lu_{0.1875}N$ 结构1;(j) $Ga_{0.8125}Lu_{0.1875}N$ 结构2;(k) $Ga_{0.8125}Lu_{0.1875}N$ 结构3;(l) $Ga_{0.8125}Lu_{0.1875}N$ 结构4;(m) $Ga_{0.8125}Lu_{0.1875}N$ 结构5;(n) $Ga_{0.8125}Lu_{0.1875}N$ 结构6;(o) $Ga_{0.75}Lu_{0.25}N$

Fig. 2　Supercell structures (blue dots present N atoms, brown dots present Ga atoms, and green dot presents Lu atom). (a) Primitive cell of GaN; (b) GaN supercell; (c) $Ga_{0.9375}Lu_{0.0625}N$; (d) $Ga_{0.875}Lu_{0.125}N$ structure 1; (e) $Ga_{0.875}Lu_{0.125}N$ structure 2; (f) $Ga_{0.875}Lu_{0.125}N$ structure 3; (g) $Ga_{0.875}Lu_{0.125}N$ structure 4; (h) $Ga_{0.875}Lu_{0.125}N$ structure 5; (i) $Ga_{0.8125}Lu_{0.1875}N$ structure 1; (j) $Ga_{0.8125}Lu_{0.1875}N$ structure 2; (k) $Ga_{0.8125}Lu_{0.1875}N$ structure 3; (l) $Ga_{0.8125}Lu_{0.1875}N$ structure 4; (m) $Ga_{0.8125}Lu_{0.1875}N$ structure 5; (n) $Ga_{0.8125}Lu_{0.1875}N$ structure 6; (o) $Ga_{0.75}Lu_{0.25}N$;

表1　优化后GaN和Lu掺杂GaN体系参数值

Table 1　Parameters of pure and Lu doped GaN after optimization

Model	a, b /nm	c /nm	V /nm^3	E /eV	E_f /eV	E_b /eV
GaN (experimental)[45]	0.3189	0.5185	—	—	—	
GaN (calculated)	0.3171	0.5149	0.3587	−38796.821	—	−5.782
$Ga_{0.9375}Lu_{0.0625}N$	0.3211	0.5210	0.3658	−43750.583	0.207	−5.602
$Ga_{0.875}Lu_{0.125}N$ structure 1	0.3239	0.5257	0.3819	−48706.936	−2.177	−5.677
$Ga_{0.875}Lu_{0.125}N$ structure 2	0.3242	0.5248	0.3820	−48707.119	−2.360	−5.682
$Ga_{0.875}Lu_{0.125}N$ structure 3	0.3240	0.5244	0.3817	−48707.024	−2.265	−5.679
$Ga_{0.875}Lu_{0.125}N$ structure 4	0.3242	0.5240	0.3822	−48706.943	−2.184	−5.676
$Ga_{0.875}Lu_{0.125}N$ structure 5	0.3246	0.5244	0.3818	−48707.023	−2.265	−5.678
$Ga_{0.8125}Lu_{0.1875}N$ structure 1	0.3267	0.5308	0.3923	−53663.363	−4.635	−5.754
$Ga_{0.8125}Lu_{0.1875}N$ structure 2	0.3287	0.5271	0.3923	−53663.360	−4.632	−5.753
$Ga_{0.8125}Lu_{0.1875}N$ structure 3	0.3282	0.5271	0.3922	−53663.604	−4.876	−5.761
$Ga_{0.8125}Lu_{0.1875}N$ structure 4	0.3277	0.5286	0.3923	−53663.492	−4.764	−5.758
$Ga_{0.8125}Lu_{0.1875}N$ structure 5	0.3283	0.5265	0.3923	−53663.787	−5.059	−5.767
$Ga_{0.8125}Lu_{0.1875}N$ structure 6	0.3277	0.5281	0.3919	−53663.604	−4.876	−5.753
$Ga_{0.75}Lu_{0.25}N$	0.3294	0.5363	0.4029	−58620.005	−7.308	−5.837

12.5% 和 18.75% 时的 Lu 掺杂对 GaN 的影响。

3.2 电子结构

为方便比较各个体系的能带结构与态密度，均选取 $E=0$ eV 作为费米能级。本征 GaN 的能带结构和态密度如图 3 所示，从图 3(a)中可以看出，导带底和价带顶位于布里渊区高对称点，体系为直接带隙半导体，且禁带宽度为 3.42 eV，这与实验值 3.40 eV 符合得很好，误差仅为 0.59%。由图 3(b)可知：费米能级附近 Ga 的 4p 态和 N 的 2p 态以及少量的 Ga 的 3d 态对体系的贡献较大；在 0～4 eV 内，Ga、N 原子电子组态对体系几乎没有贡献，这与能带图相符合；在 −4～0 eV 内，Ga 的 4s4p 态以及少量 N 的 2p 态对体系的贡献较大。

掺杂后 GaN 体系的能带结构如图 4 所示。从图 4 中可以看出，掺杂后体系价带导带数目明显变多，在费米能级附近产生了杂质带。掺杂后体系的自旋向上和

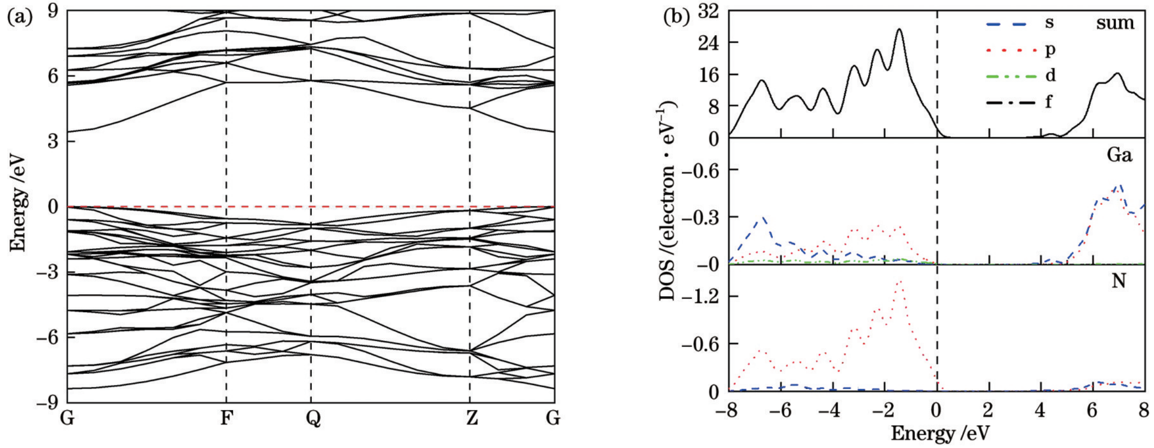

图 3 本征 GaN 能带结构和态密度(DOS)。(a)能带结构；(b) DOS

Fig. 3 Band structures and DOS of ideal GaN. (a) Band structures; (b) DOS

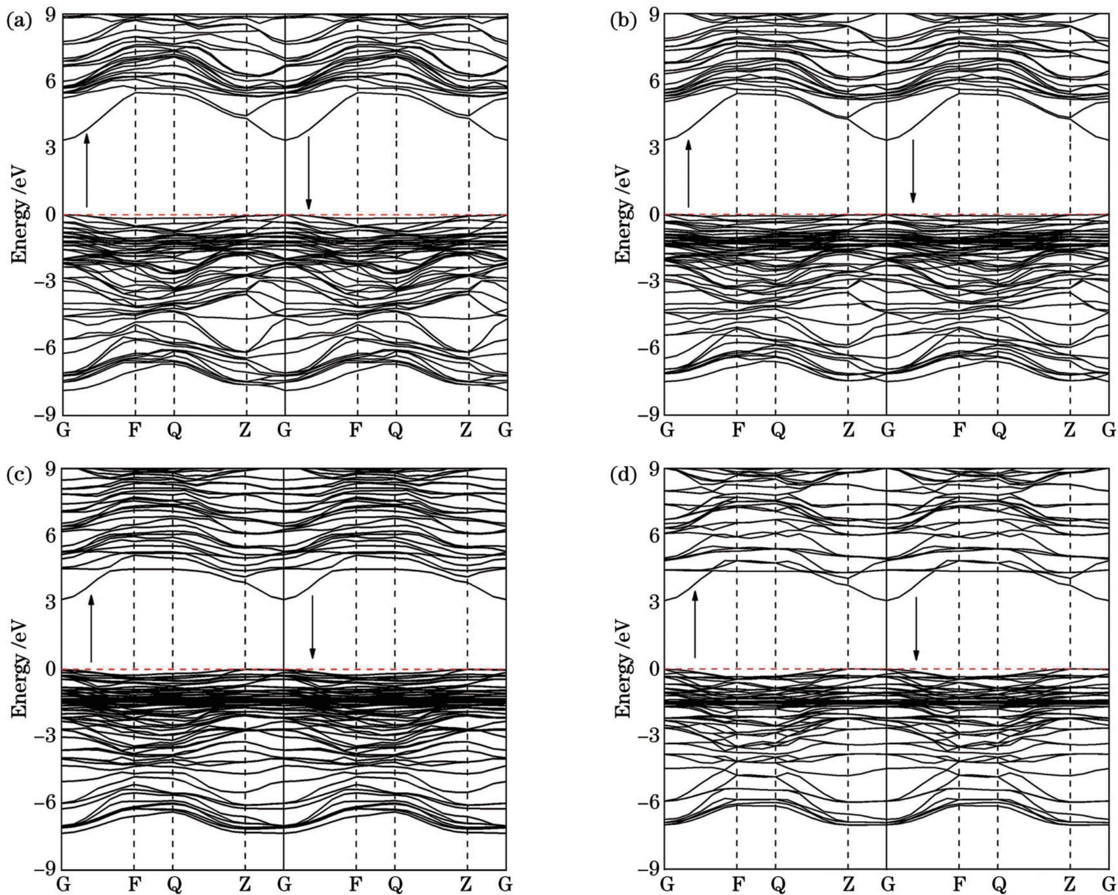

图 4 掺杂 GaN 体系能带结构。(a) $Ga_{0.9375}Lu_{0.0625}N$；(b) $Ga_{0.875}Lu_{0.125}N$；(c) $Ga_{0.8125}Lu_{0.1875}N$；(d) $Ga_{0.75}Lu_{0.25}N$

Fig. 4 Band structures of doped GaN. (a) $Ga_{0.9375}Lu_{0.0625}N$; (b) $Ga_{0.875}Lu_{0.125}N$; (c) $Ga_{0.8125}Lu_{0.1875}N$; (d) $Ga_{0.75}Lu_{0.25}N$

自旋向下能带结构完全对称，说明掺杂体系为非磁性材料。不同掺杂浓度下Lu掺杂GaN体系均显现为直接带隙P型半导体特征，且禁带宽度均有所减小。当掺杂浓度为18.75%和25%时，体系在价带顶附近产生杂质能级。不同掺杂浓度下$Ga_{1-x}Lu_xN$（x=0.0625、0.125、0.1875、0.25）体系带隙分别减小为3.34 eV、3.24 eV、3.13 eV、3.06 eV。带隙减小则有利于电子的跃迁，从而有助于提升体系的光学性能。图5为不同掺杂浓度下Lu掺杂GaN的态密度图。从图5中可以直观地观察到，掺杂体系中Ga的4p态、N的2p态以及Lu的4f态对费米能级对体系的贡献很大。掺杂后体系费米能级均穿过价带，为P型半导体。

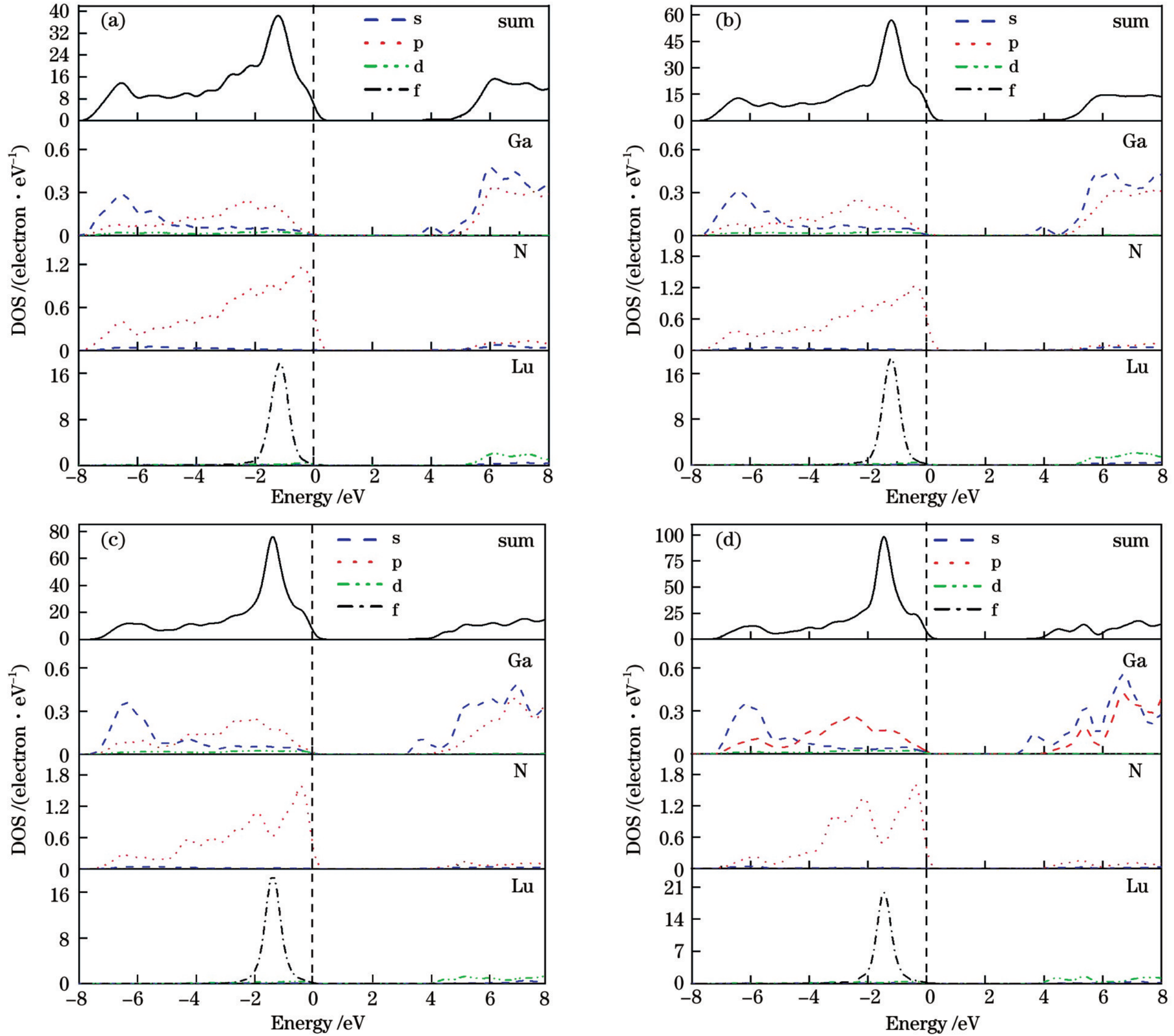

图5 掺杂GaN体系态密度。(a) $Ga_{0.9375}Lu_{0.0625}N$；(b) $Ga_{0.875}Lu_{0.125}N$；(c) $Ga_{0.8125}Lu_{0.1875}N$；(d) $Ga_{0.75}Lu_{0.25}N$

Fig. 5 DOS of doped GaN. (a) $Ga_{0.9375}Lu_{0.0625}N$; (b) $Ga_{0.875}Lu_{0.125}N$; (c) $Ga_{0.8125}Lu_{0.1875}N$; (d) $Ga_{0.75}Lu_{0.25}N$

3.3 光学性质

在光响应范围内，半导体材料的宏观光学性质可以用介电函数来表示，通过直接跃迁概率定义和Kramers-Kronig色散关系，可以推导出半导体介电函数的实部和虚部[46]为

$$\varepsilon_1(\omega)=1+\frac{2}{\pi}\rho_0\int_0^{\infty}\frac{\omega'\varepsilon_2(\omega)}{\omega'^2-\omega^2}\mathrm{d}\omega, \tag{3}$$

$$\varepsilon_2(\omega)=\frac{A}{\omega^2}\sum_{\mathrm{C,V}}\int_{\mathrm{BZ}}\frac{1}{\pi^3}\left|M_{\mathrm{CV}}(K)\right|^2\times \delta\left(E_{\mathrm{C}}^K-E_{\mathrm{V}}^K-h\omega\right)\mathrm{d}^3K, \tag{4}$$

式中：下标C、V分别表示导带和价带；下标BZ表示第一布里渊区；K为倒格矢；A为常数；$\left|M_{\mathrm{CV}}(K)\right|^2$为动量矩阵元；$\omega$为圆周频率；$E_{\mathrm{C}}^K$、$E_{\mathrm{V}}^K$分别为导带、价带的本征能级。

图6为掺杂前后GaN体系的介电函数实部和虚部。从图6(a)中可以看出，本征GaN的静介电常数为4.50，略低于实验值[47]。不同掺杂浓度的Lu掺杂后静介电常数均有所增大，当掺杂浓度为25%时，GaN的静介电常数从4.50增加至5.42，这一提高有助于增强电子器件的储能能力[48]。介电函数的虚部可以表征电子跃迁的数目，由图6(b)可知，本征GaN在光子能量

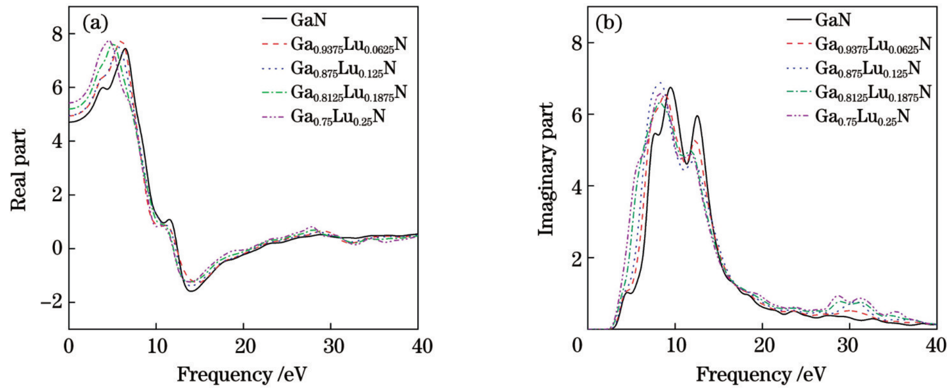

图 6　GaN 和 Lu 掺杂 GaN 体系的介电函数实部和虚部。(a)实部；(b)虚部

Fig. 6　Real and imaginary parts of dielectric function in GaN and Lu doped GaN. (a) Real part; (b) imaginary part

为 9.25 eV 时出现强峰，峰值为 6.26，在 12.60 eV 时出现次强峰，对应于 Ga 原子 4s 态的跃迁。不同掺杂浓度下掺杂后 $Ga_{1-x}Lu_xN$(x=0.0625、0.125、0.1875、0.25)体系的强峰分别左移至 8.85 eV、8.38 eV、8.28 eV、8.06 eV，发生了红移。

半导体的吸收系数 $\alpha(\omega)$ 可表示为

$$\alpha(\omega)=\frac{\sqrt{2}\,\omega}{c}\left\{\left[\varepsilon_1(\omega)^2+\varepsilon_2(\omega)^2\right]^{1/2}-\varepsilon_1(\omega)\right\}^{\frac{1}{2}}。\quad(5)$$

计算得到 GaN 掺杂前后的吸收谱如图 7 所示。从图 7(a)中可以看出，本征 GaN 的吸收带边为 3.25 eV，接近实验结果(3.29 eV)[23]。当掺杂浓度为 6.25%、12.5%、18.75% 和 25% 的 Lu 掺杂后光吸收带边分别左移至 3.17eV、3.09 eV、2.53 eV、2.18 eV，发生红移，说明结构对光的响应能力有所提高。不同掺杂浓度下 Lu 掺杂后，25～40 eV 区域内产生新的次强峰，该峰来自 Lu 的 4f 态电子轨道杂化，价带与导带之间形成了新的局域杂质能级，从而实现电子从价带顶到杂质能级、杂质能级到导带底的跃迁，这增强了 GaN 的光谱响应强度。掺杂前后可见光区域(300～800 nm)的吸收光谱如图 7(b)所示，由图可知，本征 GaN 在可见光范围内的吸收系数较小，对可见光的利用率低，当掺杂浓度为 25% 时，$Ga_{0.75}Lu_{0.25}N$ 体系形成了较宽的可见光吸收区域，可见 Lu 掺杂提升了 GaN 的光催化性能。

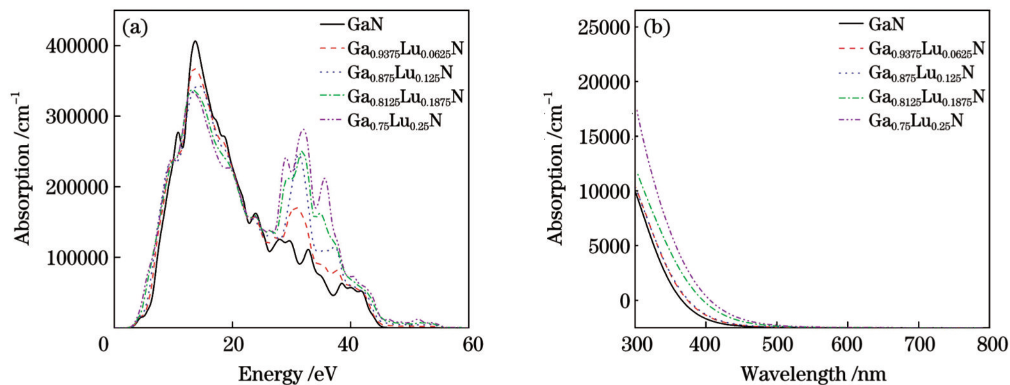

图 7　GaN 和 Lu 掺杂的 GaN 体系的吸收。(a)光子能量；(b)波长

Fig. 7　Absorption of GaN and Lu doped GaN systems. (a) Photon energy; (b) wavelength

能量损失谱可以表示电子在穿越材料时的能量损失，体系的能量损失函数 $L(\omega)$ 为

$$L(\omega)=\frac{\varepsilon_2(\omega)}{\varepsilon_1^2(\omega)+\varepsilon_2^2(\omega)}。\quad(6)$$

图 8 为不同掺杂浓度下 Lu 掺杂 GaN 体系的能量损失函数。从图中可以看出，掺杂后体系能量损失最大值均有所降低，且峰值相对左移。

4　结　　论

采用基于密度泛函理论的第一性原理方法，计算了不同掺杂浓度 $Ga_{1-x}Lu_xN$(x=0.0625、0.125、0.1875、0.25)体系的能带结构、态密度和光学性质。结果表明：掺杂后各体系结构稳定，晶格常数发生畸变，体积有所增大。掺杂后的 GaN 仍为直接带隙 P 型半导体，Lu 的掺入诱导了浅能级杂质，使得各掺杂浓度的掺杂体系带隙均有所减小，且在费米能级附近产生杂质能级，该能级主要来自 Lu 原子的 4f 态和 5d 态。与本征 GaN 相比，当 Lu 的掺杂浓度为 25% 时，GaN 的静介电常数从 4.50 增加至 5.42。掺杂后 GaN 体系的介电函数虚部往低能方向移动，能量最大损失值有所降

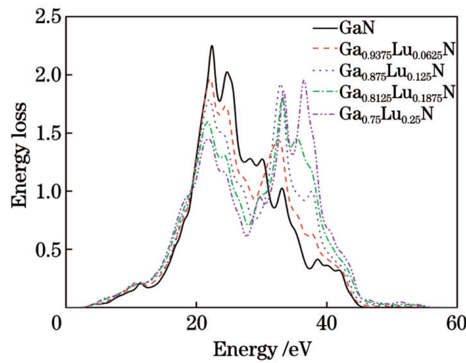

图 8 GaN和Lu掺杂的GaN体系的能量损失谱

Fig. 8 Energy loss for GaN and Lu doped GaN

低，光吸收带边发生了红移现象，吸收光谱范围增大，GaN 的光催化性能得到增强。计算结果为稀土元素 Lu 掺杂 GaN 高压光电材料的器件研究提供了理论参考。

参 考 文 献

[1] Levinshtein M E, Rumyantsev S L, Shur M S. Properties of advanced semiconductor materials: GaN, AlN, InN, BN, SiC, SiGe[M]. New York: Wiley, 2001.

[2] Rais-Zadeh M, Gokhale V J, Ansari A, et al. Gallium nitride as an electromechanical material[J]. Journal of Microelectromechanical Systems, 2014, 23(6): 1252-1271.

[3] Dadgar A, Hempel T, Bläsing J, et al. Improving GaN-on-silicon properties for GaN device epitaxy[J]. Physica Status Solidi C, 2011, 8(5): 1503-1508.

[4] Harima H. Properties of GaN and related compounds studied by means of Raman scattering[J]. Journal of Physics: Condensed Matter, 2002, 14(38): R967-R993.

[5] Pearton S J. GaN and related materials II[M]. London: CRC Press, 2000.

[6] Asad M, Li Q, Lee C H, et al. Integration of GaN light-emitting diodes with a-Si: H thin-film transistors for flexible displays[J]. Nanotechnology, 2019, 30(32): 324003.

[7] Kim T I, Jung Y H, Song J Z, et al. High-efficiency, microscale GaN light-emitting diodes and their thermal properties on unusual substrates[J]. Small, 2012, 8(11): 1643-1649.

[8] Behringer M, König H. Blue high-power laser diodes: beam sources for novel applications: overview and outlook[J]. PhotonicsViews, 2020, 17(2): 60-63.

[9] Nam O H, Ha K H, Kwak J S, et al. Characteristics of GaN-based laser diodes for post-DVD applications[J]. Physica Status Solidi (a), 2004, 201(12): 2717-2720.

[10] Keshmiri N, Wang D Q, Agrawal B, et al. Current status and future trends of GaN HEMTs in electrified transportation[J]. IEEE Access, 2020, 8: 70553-70571.

[11] Mishra U K, Parikh P, Wu Y F. AlGaN/GaN HEMTs: an overview of device operation and applications[J]. Proceedings of the IEEE, 2002, 90(6): 1022-1031.

[12] Babichev A V, Zhang H, Lavenus P, et al. GaN nanowire ultraviolet photodetector with a graphene transparent contact[J]. Applied Physics Letters, 2013, 103(20): 201103.

[13] 李金晓, 刘震, 叶思灿, 等. P-I-N 型 GaN 紫外探测器的正向电流输运[J]. 激光与光电子学进展, 2023, 60(23): 2304002.
Li J X, Liu Z, Ye S C, et al. Forward current transport in P-I-N type GaN ultraviolet detector[J]. Laser & Optoelectronics Progress, 2023, 60(23): 2304002.

[14] Gundimeda A, Krishna S, Aggarwal N, et al. Fabrication of non-polar GaN based highly responsive and fast UV photodetector[J]. Applied Physics Letters, 2017, 110(10): 103507.

[15] Zhuo R R, Zeng L H, Yuan H Y, et al. *In-situ* fabrication of $PtSe_2$/GaN heterojunction for self-powered deep ultraviolet photodetector with ultrahigh current on/off ratio and detectivity [J]. Nano Research, 2019, 12(1): 183-189.

[16] Cao D Z, Xiao H D, Xu H Z, et al. Enhancing the photocatalytic activity of GaN by electrochemical etching[J]. Materials Research Bulletin, 2015, 70: 881-886.

[17] Jung H S, Hong Y J, Li Y R, et al. Photocatalysis using GaN nanowires[J]. ACS Nano, 2008, 2(4): 637-642.

[18] Ren B F, Zhang X L, Zhao M, et al. Significant enhancement in photocatalytic activity of $(GaN)_{1-x}(ZnO)_x$ nanowires via solubility and crystal facet tailoring[J]. AIP Advances, 2018, 8 (1): 015206.

[19] Arakawa Y, Ueno K, Imabeppu H, et al. Electrical properties of Si-doped GaN prepared using pulsed sputtering[J]. Applied Physics Letters, 2017, 110(4): 042103.

[20] 唐道胜, 华钰超, 周艳光, 等. GaN 薄膜的热导率模型研究[J]. 物理学报, 2021, 70(4): 045101.
Tang D S, Hua Y C, Zhou Y G, et al. Thermal conductivity modeling of GaN films[J]. Acta Physica Sinica, 2021, 70(4): 045101.

[21] Ho V X, Wang Y, Ryan B, et al. Observation of optical gain in Er-doped GaN epilayers[J]. Journal of Luminescence, 2020, 221: 117090.

[22] 胡磊, 张立群, 刘建平, 等. 高功率氮化镓基蓝光激光器[J]. 中国激光, 2020, 47(7): 0701025.
Hu L, Zhang L Q, Liu J P, et al. High power GaN-based blue lasers[J]. Chinese Journal of Lasers, 2020, 47(7): 0701025.

[23] Tetsuo N, Nobuyuki I, Kazuyoshi T, et al. Wide range doping control and defect characterization of GaN layers with various Mg concentrations[J]. Journal of Applied Physics, 2018, 124 (16): 165706.

[24] Kozodoy P, Xing H L, DenBaars S P, et al. Heavy doping effects in Mg-doped GaN[J]. Journal of Applied Physics, 2000, 87(4): 1832-1835.

[25] Polyakov A Y, Smirnov N B, Govorkov A V, et al. Properties of Fe-doped semi-insulating GaN structures[J]. Journal of Vacuum Science & Technology B: Microelectronics and Nanometer Structures Processing, Measurement, and Phenomena, 2004, 22(1): 120-125.

[26] Su H K, Xu S R, Tao H C, et al. Improving the current spreading by Fe doping in n-GaN layer for GaN-based ultraviolet light-emitting diodes[J]. IEEE Electron Device Letters, 2021, 42(9): 1346-1349.

[27] Zeng C H, Lin W K, He T, et al. Ultraviolet-infrared dual-color photodetector based on vertical GaN nanowire array and graphene[J]. Chinese Optics Letters, 2020, 18(11): 112501.

[28] Maskar E, Lamrani A F, Belaiche M, et al. Electronic, magnetic, optical and transport properties of wurtzite-GaN doped with rare earth (RE=Pm, Sm, and Eu): first principles approach[J]. Surfaces and Interfaces, 2021, 24: 101051.

[29] Eisa M H. Electronic structure and optical properties of Cd co-doped wurtzite GaN exposed from first principles study[J]. Results in Physics, 2019, 13: 102330.

[30] Lantri M, Boukortt A, Meskine S, et al. Effect of erbium doping on GaN electronic and optical properties: first-principles study[J]. Modern Physics Letters B, 2019, 33(27): 1950327.

[31] Khan M J I, Kanwal Z, Latif A, et al. Investigations on electronic structure, magnetic and optical properties of C and Ti co-doped zincblende GaN for optoelectronic applications[J]. Optik, 2021, 231: 166425.

[32] Shen P F, Li E L, Zhang L, et al. Electronic structures and physical properties of Mg, C, and S doped g-GaN[J]. Superlattices and Microstructures, 2021, 156: 106930.

[33] Belhachi S, Lazreg A, Dridi Z, et al. Electronic and magnetic investigations of rare-earth Tm-doped AlGaN ternary alloy[J]. Journal of Superconductivity and Novel Magnetism, 2018, 31(6): 1767-1771.

[34] Hoang K. Rare-earth defects in GaN: a systematic investigation of the lanthanide series[J]. Physical Review Materials, 2022, 6(4): 044601.

[35] Lo F Y, Huang C D, Chou K C, et al. Structural, optical, and magnetic properties of highly-resistive Sm-implanted GaN thin films[J]. Journal of Applied Physics, 2014, 116(4): 043909.

[36] Melton A G, Liu Z Q, Kucukgok B, et al. Properties of MOCVD-grown GaN:Gd films for spintronic devices[J]. MRS Online Proceedings Library, 2012, 1396(1): 164-168.

[37] Wang S, Xie X J, Liu H, et al. Structural and magnetic properties of Dy-implanted GaN films[J]. Journal of Alloys and Compounds, 2017, 712: 482-485.

[38] Kohn W, Becke A D, Parr R G. Density functional theory of electronic structure[J]. The Journal of Physical Chemistry, 1996, 100(31): 12974-12980.

[39] Zakrzewski T, Boguslawski P. Electronic structure of transition metal ions in GaN and AlN: comparing GGA+U with experiment[J]. Journal of Alloys and Compounds, 2016, 664: 565-579.

[40] Larson P, Lambrecht W R L, Chantis A, et al. Electronic structure of rare-earth nitrides using the LSDA+U approach: importance of allowing 4f orbitals to break the cubic crystal symmetry[J]. Physical Review B, 2007, 75(4): 045114.

[41] Monkhorst H J, Pack J D. Special points for Brillouin-zone integrations[J]. Physical Review B, 1976, 13(12): 5188-5192.

[42] 张栌丹，王明文，刘世香，等. 基质掺杂离子对(Y, Rn)$_2$O$_2$S: Sm^{3+}, Ti^{4+}, Mg^{2+}(Rn=La, Gd, Lu, Ga, Al)红色长余辉材料余辉性能的影响[J]. 工程科学学报, 2008, 30(1): 49-52.
Zhang L D, Wang M W, Liu S X, et al. Effect of host-doping ions on the afterglow property of (Y, Rn)$_2$O$_2$S: Sm^{3+}, Ti^{4+}, Mg^{2+} (Rn=La, Gd, Lu, Ga, Al) red phosphors[J]. Chinese Journal of Engineering, 2008, 30(1): 49-52.

[43] Cui X Y, Medvedeva J E, Delley B, et al. Spatial distribution and magnetism in poly-Cr-doped GaN from first principles[J]. Physical Review B, 2007, 75(15): 155205.

[44] Xiong Z H, Jiang F Y, Wan Q X, et al. Influence of crystal structure and formation energies of impurities (Mg, Zn and Ca) in zinc blende GaN[J]. Transactions of Nonferrous Metals Society of China, 2006, 16: s854-s857.

[45] Maruska H P, Tietjen J J. The preparation and properties of vapor-deposited single-crystal-line GaN[J]. Applied Physics Letters, 1969, 15(10): 327-329.

[46] Brown G F, Wu J. Third generation photovoltaics[J]. Laser & Photonics Reviews, 2009, 3(4): 394-405.

[47] Pankove J I, Berkeyheiser J E, Maruska H P, et al. Luminescent properties of GaN[J]. Solid State Communications, 1970, 8(13): 1051-1053.

[48] Gao J H, Wang Y, Liu Y B, et al. Enhancing dielectric permittivity for energy-storage devices through tricritical phenomenon[J]. Scientific Reports, 2017, 7: 40916.

First Principles Study on Electronic Structure and Optical Properties of Lu Doped GaN at Different Doping Concentration

Fu Shasha, Xiao Qingquan*, Tang Huazhu, Yao Yunmei, Zou Mengzhen, Ye Jianfeng, Xie Quan

Institute of Advanced Optoelectronic Materials and Technology, College of Big Data and Information Engineering, Guizhou University, Guiyang 550025, *Guizhou, China*

Abstract

Objective As a third-generation novel semiconductor material emerging alongside SiC, GaN has become a hot topic in the fields of high-temperature and high-power microwave devices, laser devices, and optoelectronic devices due to its excellent characteristics. It has been widely used in microwave communication, lasers, detectors, and ultraviolet light-emitting diodes. Doping, as a new paradigm for material modification, can directly and effectively control and improve the thermoelectric, photoelectric, and magnetic properties of materials, giving them new characteristics and extending their applications. Materials based on rare earth elements have excellent optical, electrical, magnetic, and catalytic properties, and are the foundation for building various new functional materials. It is expected that rare earth element doping can improve GaN's visible light absorption. We study the electronic structures and optical properties of GaN doped with different concentrations (atomic number fraction) of Lu using the first-principles plane wave ultrasoft pseudopotential method. The calculation results provide theoretical support for the development of device applications of GaN semiconductor photoelectric materials doped with rare earth element Lu.

Methods We adopt the CASTEP software package using the first-principles calculation method based on the density functional theory. We utilize the projected augmented wave method as the pseudo potential and apply the generalized gradient approximation function proposed by Perdew-Burke-Ernzerhof to express the exchange correlation interaction. We adopt the plane wave expansion with a cut-off energy of 450 eV and leverage the conjugate gradient method to optimize the lattice constants and atom positions of the diverse models. The K-point grid in the Monkhorst-Pack form is set as $4\times 4\times 2$ for bulk models. As the GGA method underestimates the band gap value of materials, we use the GGA+U plane

wave pseudopotential method to correct the band gap. A supercell model with 2×2×2 is built, including 16 Ga atoms and 16 N atoms, with a total of 32 atoms. To make the calculation results more accurate, we conduct a truncation energy convergence test on the supercell systems. Considering the symmetry of GaN crystal, we study the stability of different spatial ordered configurations with the same doping amount at concentrations of 12.5% and 18.75%.

Results and Discussions From the formation energy (Table 1), it can be seen that except for the $Ga_{0.9375}Lu_{0.0625}N$ system, which has a higher formation energy, the values of the formation energy and binding energy of other doping systems are all negative, indicating that doping enhances the structural stability of intrinsic GaN. The formation energy of the $Ga_{0.9375}Lu_{0.0625}N$ system has a positive value, making it more challenging to achieve doping compared to other doping concentrations. Under different concentrations, the Lu-doped GaN systems show direct band gap P-type semiconductor characteristics (Fig. 4), and the band gaps are all narrowed. The reduction of band gap is beneficial for electron transition, thereby improving the optical properties of the GaN system. The absorption edges of Lu-doped GaN under four concentrations show a red shift phenomenon (Fig. 7), indicating an improvement in light response capability. The intrinsic GaN has a small absorption coefficient in the visible light range and has low utilization of visible light. When the doping concentration of Lu is 25%, the $Ga_{0.75}Lu_{0.25}N$ system forms a wider visible light absorption region.

Conclusions We calculate the electronic structures and optical properties of intrinsic GaN and Lu-doped $Ga_{1-x}Lu_xN$ (x=0.0625, 0.125, 0.1875, 0.25) at different doping concentrations using the first-principles plane wave ultrasoft pseudopotential method under density functional theory. In addition, we study the stability of the same doping and different spatially ordered occupancy architectures when the Lu doping concentration is 12.5% and 18.75%. The calculation results show that the values of lattice parameters of the Lu-doped GaN are increased, and the band gap values of the doped GaN are reduced compared to the intrinsic band gap (3.40 eV) due to the shallow energy level impurities induced by the doping of Lu. Compared with the intrinsic GaN, the static dielectric constants of the Lu-doped GaN increase and even reach 5.42 when the doping concentration of Lu is 25%. The imaginary parts of the dielectric function and the absorption spectrum of the Lu-doped GaN shift in the low-energy direction. The red-shift phenomenon occurs which extends the absorption spectral range and enhances the photocatalytic performance of GaN.

Key words materials; gallium nitride; substitution doping; electronic structure; optical properties